AIAA JOURNAL
Vol. 46, No. 2, February 2008

Global Luminescent Oil-Film Skin-Friction Meter

Tianshu Liu,* J. Montefort,† S. Woodiga,‡ and P. Merati§
Western Michigan University,
Kalamazoo, Michigan 49008
and
Lixin Shen¶
Syracuse University, Syracuse, New York 13244

DOI: 10.2514/1.32219

This paper describes a global luminescent oil-film skin-friction meter that is particularly useful in global skin-friction diagnostics for complex flows. This method is developed based on the relationship between the oil-film thickness and luminescent intensity of an oil film doped with luminescent molecules. The projected thin oil-film equation is given in the image plane, which relates skin friction with the normalized luminescent intensity. A variational formulation with a smoothness constraint on skin friction is given, and the corresponding Euler–Langrage equations are solved to obtain a snapshot solution for a relative skin-friction field. Successive snapshot solutions are superposed to reconstruct a complete relative skin-friction field, and the corresponding absolute field can be further determined by in situ calibration. This method is examined through numerical simulation and experiments.

Nomenclature

a	=	proportional coefficient in Eq. (2)
C_f	=	skin-friction coefficient
c	=	airfoil chord
g	=	normalized luminescent intensity
g_1, g_2	=	gravity components
h	=	oil-film thickness
I	=	luminescent intensity
I_{ex}	=	excitation intensity
I_{ref}	=	reference luminescent intensity
J	=	functional
p	=	pressure
Re_c	=	Reynolds number based on airfoil chord
s	=	arc length along a skin-friction line
T	=	temperature
T_0	=	reference temperature
t	=	time
t_1, t_2	=	time scales defined in Appendix B
X_1, X_2	=	object space coordinates on surface
x_1, x_2	=	image coordinates
α	=	Lagrange multiplier
κ	=	absorptivity of luminescent molecule
λ	=	scaling factor in perspective projection
μ	=	oil viscosity
ξ	=	similarity variable defined in Appendix B
ρ	=	oil density
$\boldsymbol{\tau}$	=	skin friction
$\bar{\boldsymbol{\tau}}$	=	equivalent skin friction
τ_s	=	skin friction along a skin-friction line
Φ	=	quantum efficiency of luminescent molecule

Received 17 May 2007; revision received 15 September 2007; accepted for publication 25 September 2007.

*Corresponding Author, Associate Professor, Department of Mechanical and Aeronautical Engineering, G-220, Parkview Campus; tianshu.liu@wmich.edu. Senior Member AIAA.

†Research Assistant Professor, Department of Mechanical and Aeronautical Engineering, Parkview Campus. Member AIAA.

‡Graduate Assistant, Department of Mechanical and Aeronautical Engineering, Parkview Campus.

§Professor and Chair, Department of Mechanical and Aeronautical Engineering, Parkview Campus.

¶Assistant Professor, Department of Mathematics.

I. Introduction

SKIN friction, along with surface pressure and temperature, is one of the most important surface quantities in aerodynamics and fluid mechanics. It is also the most difficult surface quantity to measure. A variety of techniques have been developed for measurement of skin friction, and most of them are indirect and nonglobal techniques that only provide a value of skin friction at a location using a single sensing element [1–4]. Candidate techniques for global skin-friction measurement are shear sensitive liquid crystal (SSLC), surface stress sensitive film (S3F), and oil film. These techniques can be considered as direct or semidirect methods because the quantity to be detected directly responds to skin friction. Considerable effort has been made particularly by Reda of the NASA Ames Research Center to develop SSLC for quantitative skin-friction measurement [5–8]. The observables from SSLC are transient color changes that result from the change in the pitch of the helix of the cholesteric structure of SSLC due to change in mechanical stress. The data analysis using color as a parameter for measuring both the magnitude and direction of a skin-friction vector is complicated for reliable quantitative measurement. The strong dependency of reflection on both the illumination direction and viewing angle of a camera makes universal system calibration difficult. Although SSLC has been successfully used for global skin-friction measurement in an impinging jet, the complicated calibration problem prevents existing SSLC from being a routine, quantitative technique for wind-tunnel testing and other practical measurements. Surface stress sensitive film is a relatively new technique for global skin-friction measurement, which combines a particle-imaging-velocimetry-like (PIV) correlation technique and fluorescence for measuring a deformation field of a specific polymeric film in flow [9,10]. The polymeric film is doped with luminescent molecules and seeded with tracer particles. Skin friction and pressure are simultaneously extracted from the tangential and normal components of deformation based on a certain system model because S3F is sensitive to both skin friction and pressure. For good control of film thickness, a cavity on a model or a flexible layer that can be glued on a model is needed to form a polymeric film. This special requirement may limit the application of S3F in production wind-tunnel tests in which modification of a model is not allowed.

The capability of S3F has been demonstrated in several flows to measure the complicated topological structures of skin-friction fields.

The oil-film skin-friction meter, invented by Tanner and Blows [11], is based on detecting temporal-spatial evolution of the thickness of a thin oil film to determine skin friction. A laser interferometer has been used to measure the thickness of a thin oil film at a particular location [12,13]. Image-based interferometers for oil-film measurements have been also developed [14–16]. As indicated in a review by Naughton and Sheplak [3], image-based interferometric oil-film meters have been used for points, lines, and regions of surface when the local relationship between skin friction and oil-film evolution can be used for oil droplets distributed on a surface. Brown and Naughton [17] have attempted to recover a global skin-friction field as an inverse problem by solving the oil-film equation on an oil-film domain. However, because one equation for the oil-film thickness is not sufficient for two unknown components of skin friction, the direction of skin friction must be known to solve the equation for the skin-friction magnitude. The present study gives a different perspective; the inverse problem for determining a skin-friction field is treated as a variational problem with a smoothness constraint.

This work is a global extension of a luminescent oil-film skin-friction meter originally proposed by Liu and Sullivan [18]. The luminescent oil is silicone oil doped with luminescent molecules. Because the luminescent intensity is proportional to the oil-film thickness for a thin oil film, thickness measurement is converted to luminescence measurement that is much easier and more robust against noise. When the oil-film thickness is transformed to the image intensity, the thin oil-film equation can be projected onto the image plane to provide a relationship between skin friction and the temporal and spatial derivatives of the image intensity. To solve the projected thin oil-film equation for skin friction, a variational formulation is given with a regularization term for the smoothness of a skin-friction field. The corresponding Euler–Lagrange equations are given with the Neumann condition, and an algorithm is developed to solve the Euler–Lagrange equations for a snapshot solution of a skin-friction field. Next, a complete relative skin-friction field is reconstructed through fusion of snapshot solutions. Without a priori calibration, this method gives a relative skin-friction field. The absolute skin-friction field can be obtained by in situ calibration using the accurate values given by a reliable point-based method at one or several locations. Simulation and experiments in several typical flows are conducted to examine this method.

II. Projected Thin Oil-Film Equation and Variational Formulation

The governing equation, which describes the response of a thin oil film on a surface $X_3 = S(X_1, X_2)$ to the externally applied three-dimensional aerodynamic flow, is given in a form of the summation convention [15,17]

$$\frac{\partial h}{\partial t} + \frac{\partial}{\partial X_i}\left[\frac{\tau_i h^2}{2\mu} - \left(\frac{\partial p}{\partial X_i} - \rho g_i\right)\frac{h^3}{3\mu}\right] = 0, \qquad (i = 1, 2) \quad (1)$$

where h is the oil-film thickness, $\boldsymbol{\tau} = (\tau_1, \tau_2)$ is the skin-friction vector, p is the pressure, μ is the oil viscosity, ρ is the oil density, and (g_1, g_2) is the gravity vector. When a thin luminescent oil film is applied to a surface, the luminescent emission intensity (radiance I) under excitation is proportional to the oil-film thickness, i.e., [18]

$$I(X_1, X_2) = aI_{\text{ex}}(X_1, X_2)h(X_1, X_2) \quad (2)$$

where $I_{\text{ex}}(X_1, X_2)$ is the intensity of the excitation light on the surface and a is a coefficient proportional to the quantum efficiency of seeded luminescent molecules and dye concentration. Substitution of Eq. (2) into Eq. (1) yields

$$\frac{\partial}{\partial t}\left(\frac{I}{I_{\text{ex}}}\right) + \frac{\partial}{\partial X_i}\left[\frac{\tau_i}{2\mu a}\left(\frac{I}{I_{\text{ex}}}\right)^2 - \left(\frac{\partial p}{\partial X_i} - \rho g_i\right)\frac{1}{3\mu a^2}\left(\frac{I}{I_{\text{ex}}}\right)^3\right] = 0, \qquad (i = 1, 2) \quad (3)$$

There is an one-to-one mapping between the image plane (x_1, x_2) and the surface $X_3 = S(X_1, X_2)$ [19]. In particular, when the image plane of a camera is parallel to a flat surface area to be measured, the perspective projection transformation $x_\beta - x_{\beta,p} = \lambda X_\beta$ $(\beta = 1, 2)$ becomes simple because the scaling factor λ is considered as a constant, where $x_{\beta,p}$ denote the principal point location in the image plane. Thus, a relation $\partial/\partial X_i = \lambda\partial/\partial x_i$ exists. For a highly curved surface, particularly near a leading edge of a wing or body, λ cannot be treated as a constant, and thus the transformation is more complicated. By introducing the normalized luminescent intensity $g = I/I_{\text{ex}}$ and the so-called equivalent skin friction $\bar{\boldsymbol{\tau}} = \boldsymbol{\tau} g(\lambda/2\mu a)$, Eq. (3) can be written in the image coordinates

$$\partial g/\partial t + \nabla(g\bar{\boldsymbol{\tau}}) = f(x_1, x_2, g) \quad (4)$$

where $\nabla = \partial/\partial x_i$ is the gradient operator in the image plane, and the effects of the pressure gradient and gravity are described by

$$f(x_1, x_2, g) = \lambda\frac{\partial}{\partial x_i}\left[\left(\lambda\frac{\partial p}{\partial x_i} - \rho g_i\right)\frac{g^3}{3\mu a^2}\right], \qquad (i = 1, 2) \quad (5)$$

Here, the measured quantity g is mapped onto the image plane. When the radiometric responsive function of a camera is linear, g equals to the normalized gray level in images. Equation (4) is a projected oil-film equation for luminescent oil film. Because of introducing the equivalent skin friction $\bar{\boldsymbol{\tau}}$, Eq. (4) has the same form as the generic projected motion equation for various flow visualizations, and the numerical method for velocity computation can be directly adopted [20]. The relative skin friction is given by $\bar{\boldsymbol{\tau}}/g$ from the equivalent skin friction.

When a spatial change of skin friction is small ($\partial\bar{\tau}_i/\partial x_i \ll 1$) and the effects of pressure gradient and gravity can be neglected ($f \ll 1$), Eq. (4) can be approximated by a simpler equation

$$\partial g/\partial t + \bar{\boldsymbol{\tau}} \cdot \nabla g = 0 \quad (6)$$

which has the same form as the optical flow constraint equation proposed by Horn and Schunck [21]. The usefulness of Eq. (6) is that it provides an initial approximation for Eq. (4) in numerical calculation.

To determine the equivalent skin-friction field $\bar{\boldsymbol{\tau}} = (\bar{\tau}_1, \bar{\tau}_2)$, Eq. (4) alone is not sufficient for determining the two unknown skin-friction components, and thus additional constraints are required. A variational formulation is given for this problem. We use a regularization term based on the L^2 norm of the skin-friction gradient that was originally proposed by Horn and Schunck [21] for computing optical flow. This smoothness condition ensures that the equivalent skin-friction field is locally continuous in all directions. This constraint is plausible at least as a first-order approximation although it is not derived based on a specific physical principle. Given g and f, a functional with the Horn–Schunck regularization term for the skin-friction field on an image domain Ω is defined as

$$J(\bar{\boldsymbol{\tau}}) = \int_\Omega [\partial g/\partial t + \nabla\cdot(g\bar{\boldsymbol{\tau}}) - f]^2\,\mathrm{d}x_1\,\mathrm{d}x_2 + \alpha\int_\Omega (|\nabla\bar{\tau}_1|^2 + |\nabla\bar{\tau}_2|^2)\,\mathrm{d}x_1\,\mathrm{d}x_2 \quad (7)$$

The Lagrange multiplier α is suitably selected. To minimize $J(\bar{\boldsymbol{\tau}})$, by introducing an arbitrary smooth function $\boldsymbol{v} = (v_1, v_2)$, computing $dJ(\bar{\boldsymbol{\tau}} + q\boldsymbol{v})/dq|_{q=0}$, and using the Green's theorem where the Neumann condition $\partial\bar{\boldsymbol{\tau}}/\partial n = 0$ is imposed on the domain boundary $\partial\Omega$, the Euler–Lagrange equations are given as follows:

$$g\frac{\partial}{\partial x_1}\left[\frac{\partial g}{\partial t}+\nabla\cdot(g\bar{\boldsymbol{\tau}})-f\right]+\alpha\nabla^2\bar{\tau}_1=0$$
$$g\frac{\partial}{\partial x_2}\left[\frac{\partial g}{\partial t}+\nabla\cdot(g\bar{\boldsymbol{\tau}})-f\right]+\alpha\nabla^2\bar{\tau}_2=0 \tag{8}$$

Similarly, for Eq. (6), the functional is

$$J(\bar{\boldsymbol{\tau}})=\int_\Omega(\partial g/\partial t+\bar{\boldsymbol{\tau}}\cdot\nabla g)^2\,\mathrm{d}x_1\,\mathrm{d}x_2+\alpha\int_\Omega(|\nabla\bar{\tau}_1|^2+|\nabla\bar{\tau}_2|^2)\,\mathrm{d}x_1\,\mathrm{d}x_2$$

and the Euler–Lagrange equations are

$$\frac{\partial g}{\partial x_1}\left[\frac{\partial g}{\partial t}+\bar{\boldsymbol{\tau}}\cdot\nabla g\right]-\alpha\nabla^2\bar{\tau}_1=0$$
$$\frac{\partial g}{\partial x_2}\left[\frac{\partial g}{\partial t}+\bar{\boldsymbol{\tau}}\cdot\nabla g\right]-\alpha\nabla^2\bar{\tau}_2=0 \tag{9}$$

Equations (8) and (9) are directly connected. To illustrate that, integrating Eq. (8) along a closed contour C in the image plane leads to

$$\oint_C\{[g_t+\nabla\cdot(g\bar{\tau})-f]\nabla g-\alpha\nabla^2\bar{\boldsymbol{\tau}}\}\cdot\mathrm{d}r=0 \tag{10}$$

Equation (10) indicates that Eq. (8) contains the solution of Eq. (9) for $\nabla\cdot\bar{\boldsymbol{\tau}}=0$ and $f=0$. Therefore, the solution of Eq. (9) can be used as an initial guess for Eq. (8) to speed up convergence. An algorithm to solve Eq. (8) is described in Appendix A. In principle, the preceding variational method can be directly applied to the thin oil-film equation, Eq. (1), when the evolution of the oil-film thickness distribution is known.

To examine the algorithm, a uniform field and an Oseen-vortex-pair field are superposed to generate a synthetic skin-friction field. The circumferential skin friction of an Oseen vortex is given by $\tau_r=(\Gamma/2\pi r)[1-\exp(-r^2/r_0^2)]$, where the vortex strength Γ and the vortex core radius r_0 are assigned. As shown in Fig. 1, a Jupiter cloud image that contains a lot of structures is used as a background oil image (g) in which the skin-friction field is artificially imposed. For testing the algorithm, the Jupiter cloud image represents an extreme case where the image intensity has abrupt changes in some regions. The temporal intensity movement in the Jupiter cloud image (g) is generated using a discretized form of Eq. (4), where a time interval between two consecutive images is 0.0001 s, f is zero, Γ is 7000, r_0 is 30 pixels, and the strength of the uniform field is 10. Figure 2 shows the skin-friction vector field and skin-friction lines recovered from two Jupiter cloud images at different instants using the proposed method. The Lagrange multipliers used in Eq. (9) for initial approximation and Eq. (8) for improvement are 1.5 and 50, respectively. Figure 3 shows a comparison between the true and recovered skin-friction distributions along the line across the cores of the vortex pair. It is observed that the large intensity variations in the Jupiter cloud images may cause some errors in the recovered results and lead to the asymmetry of the vortex pair. The calculation of skin friction is not totally immune from intrinsic large intensity variations that are not related to skin friction. This finding suggests that a smooth oil coating will improve the extracted result.

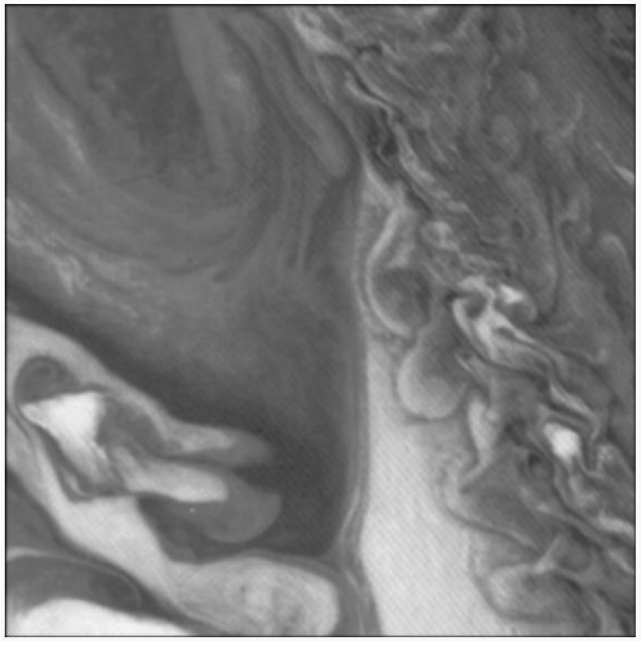

Fig. 1 Jupiter cloud image as a reference image for simulation.

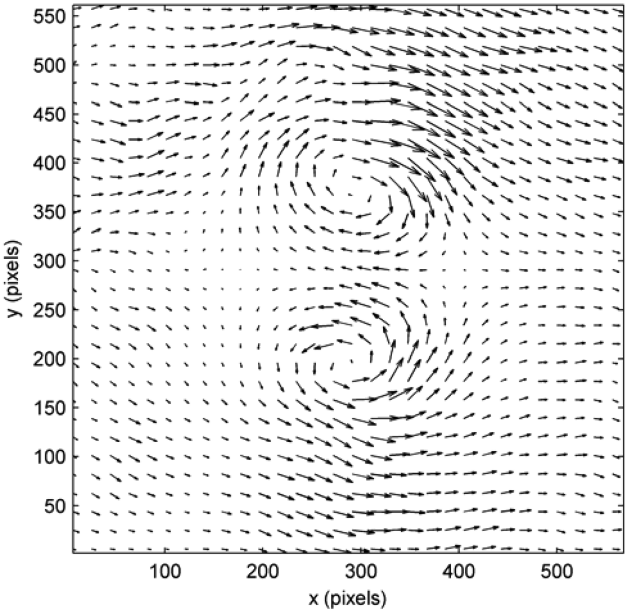

a)

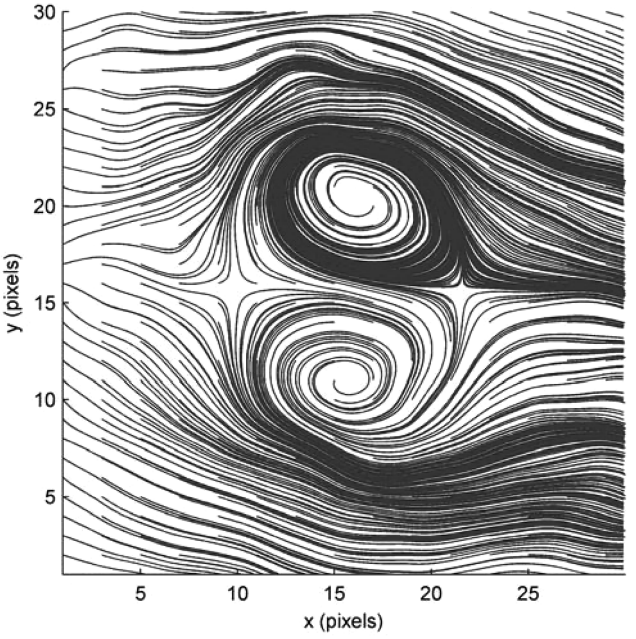

b)

Fig. 2 Skin-friction a) vector field and b) lines (at a coarser resolution for illustration) recovered from the Jupiter cloud image.

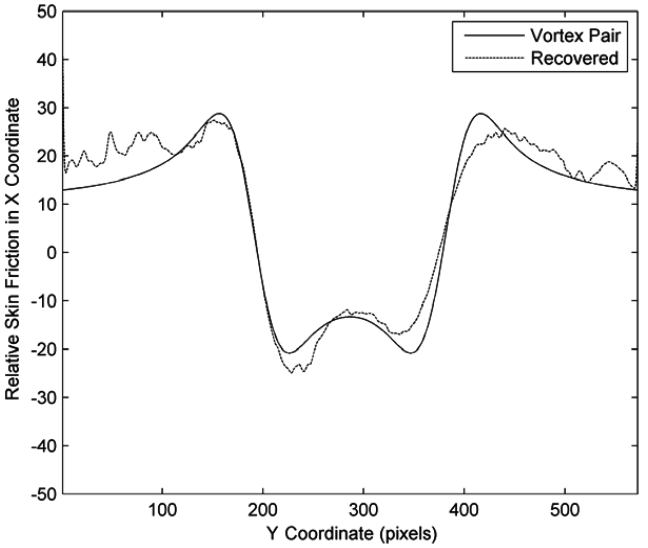

Fig. 3 Comparison between the given and recovered skin-friction distributions along the line across the cores of the vortex pair for the Jupiter cloud image.

III. Fusion of Snapshot Solutions

In fact, the preceding method gives a "snapshot" solution for a skin-friction field in a short interval between two successive images during a relatively long evolution of oil film driven by a steady-state skin-friction force. A sequence of snapshot solutions can be obtained at successive moments. Naturally, a question is whether these snapshot solutions at different moments give a unique, complete skin-friction field. Experiments indicate that, in general, these snapshot solutions may differ in magnitude and shape depending on the oil-film evolution.

To shed insight into this problem, it is first discussed whether there is a state in which snapshot solutions remain invariant and are independent from the oil-film evolution history. For the simplest case in which skin friction is constant and the effects of pressure gradient and gravity are neglected, skin friction along a skin-friction line is given by [11]

$$\tau_s = -\frac{\mu}{h}\frac{\partial h}{\partial t}\Big/\frac{\partial h}{\partial s} \tag{11}$$

where s is the coordinate along a skin-friction line. To keep τ_s independent of time, the oil-film height should be $h \propto s/t$. As indicated in Appendix B, this is a self-similar solution that is locally valid when skin friction is approximately constant in a small area. Only in the self-similar state, snapshot solutions remain the same at different moments. However, a continuous global oil-film evolution on a surface is generally in a semisimilar state depending on the time and spatial scales determined by local skin friction, temporal and spatial gradients of skin friction, and evolution distance. This semisimilarity is analogous to an intermediate asymptotics termed by Barenblatt [22]. The preceding observation is plausible after

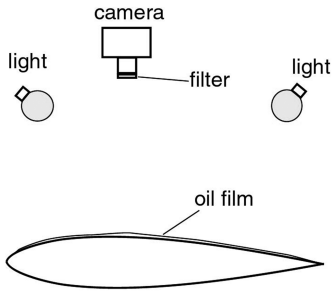

Fig. 4 Typical measurement system for luminescent oil-film skin-friction measurement.

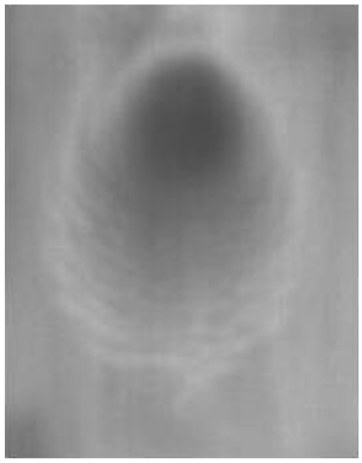

a)

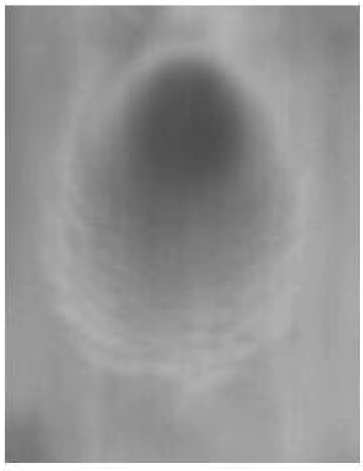

b)

Fig. 5 Typical images of luminescent oil film in the oblique impinging jet: a) 9.6 s and b) 10 s.

inspecting an approximate solution for the oil-film evolution along a skin-friction line (see Appendix B)

$$h/h_0 = \xi + (t/t_1)\xi - (t/t_2)\xi^2 + (s/s_1)\xi \tag{12}$$

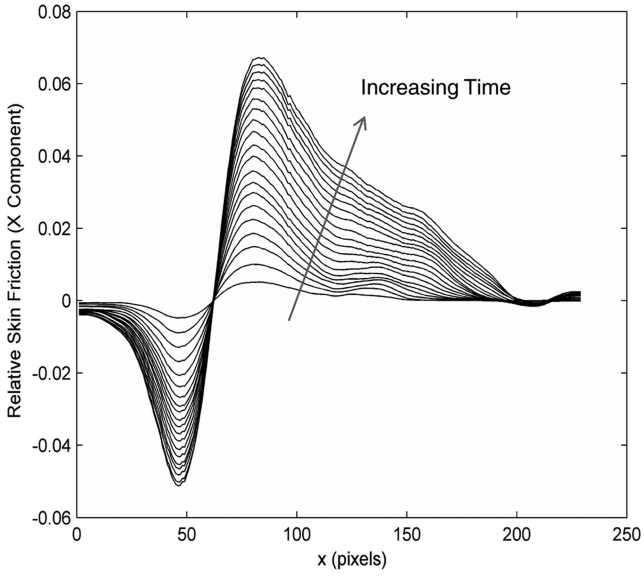

Fig. 6 The x component distributions of skin friction along the x axis (projected jet centerline) in the snapshot solutions in a time sequence with an interval of 0.4 s in the oblique impinging jet.

where the similarity variable is $\xi = \mu s/(\tau_s t h_0)$. When the time scales t_1 and t_2 and spatial scale s_1 defined in Appendix B are sufficiently large, Eq. (12) approaches to the self-similar solution $h/h_0 = \xi$. For higher skin friction and shorter evolution distance, the oil-film evolution is closer to the self-similar state, and the relaxation process is inversely proportional to skin friction. Hence, there is a spectrum of the time and spatial scales that characterize the oil-film evolution in different regions on the surface.

According to the preceding arguments, a snapshot solution captures the salient skin-friction signature in the regions where the oil-film evolution is the most sensitive to flow at that moment. Therefore, a time sequence of snapshot solutions is required to capture the major skin-friction signatures in different regions at different moments during the oil-film evolution. Then, the snapshot solutions are fused in an appropriate method to reconstruct a complete skin-friction field. A rigorous mathematical analysis for this problem is not currently available, but worthwhile to be further investigated in the future. A heuristic approach for fusion of snapshot solutions is proposed here and it is examined mainly through experiments.

A direct-fusion method is superposition of successive snapshot solutions, giving a relative skin-friction field. Another approach is a wavelet-based fusion algorithm that has three major steps. First, all snapshot skin-friction fields are decomposed using the discrete wavelet transform. Second, the wavelet coefficients of the fused skin-friction field are determined by selecting the corresponding wavelet coefficients with the largest amplitude in the snapshot fields in the transform domain, while the scaling coefficients of the fused skin-friction field are simply assigned as the averages of the corresponding low-resolution components. Finally, the fused skin-friction field is obtained using the inverse wavelet transform. In this work, Daubechies's biorthogonal wavelet filter D7/9 is used [23,24]. Tests indicate that the wavelet fusion approach is basically equivalent to the direct superposition approach in reconstruction of a complete relative skin-friction field.

IV. Absolute and Relative Skin Friction

The equivalent skin friction $\bar{\boldsymbol{\tau}}$ is determined by solving Eq. (8) numerically. The equivalent skin friction is related to the absolute skin friction by $\bar{\boldsymbol{\tau}} = \boldsymbol{\tau} g(\lambda a/2\mu)$, whereas the relative skin friction is defined by $\bar{\boldsymbol{\tau}}/g$ here. Theoretically, once the equivalent skin friction is known, the absolute skin-friction field can be obtained by $\boldsymbol{\tau} = g^{-1}(2\mu a/\lambda)\bar{\boldsymbol{\tau}}$ when the oil viscosity μ, coefficient a, scaling factor λ, and excitation light field $I_{\text{ex}}(x_1, x_2)$ are given a priori. The coefficient a in Eq. (2) is given by $a = \Phi\kappa$, where Φ and κ are the quantum efficiency and absorptivity of luminescent molecules seeded in oil, respectively. The absorptivity κ is a constant that is independent of location. However, both Φ and μ are dependent on temperature that may vary on a surface. In general, the excitation light intensity $I_{\text{ex}}(x_1, x_2)$ is nonuniform and unknown on a surface. Therefore, it is practically difficult to determine the absolute skin friction through a priori calibrations for I_{ex}, a, and μ on the surface. The following alternative method is presented.

To correct the effect of nonuniform illumination on a surface, a homogeneous luminescent reference base coating is applied on the surface. If the luminescent reference coating has a distinctly different wavelength from the luminescent oil, the emission field I_{ref} of the reference base coating can be detected using a bandpass optical filter to remove both the luminescent emission from the oil and excitation light. As indicated in Eq. (2), the emission field of the base coating under the same illumination can be described by $I_{\text{ref}} = a_{\text{ref}} I_{\text{ex}} h_{\text{ref}}$, where a_{ref} is a coefficient proportional to the quantum efficiency and concentration of the reference luminescent molecules, and the reference base coating thickness h_{ref} is a constant. Thus, the conversion relation is $I/I_{\text{ex}} = a_{\text{ref}} h_{\text{ref}} I/I_{\text{ref}}$, and the ratio I/I_{ref} is a measurable quantity. This ratioing procedure can eliminate the effect of nonuniform illumination on the surface, which is similar to the two-color method used for pressure and temperature sensitive paints (PSP and TSP) [25].

Further, substitution of $I/I_{\text{ex}} = a_{\text{ref}} h_{\text{ref}} I/I_{\text{ref}}$ into Eq. (3) leads to

$$\frac{\partial}{\partial t}\left(\frac{I}{I_{\text{ref}}}\right) + \frac{\partial}{\partial X_i}\left[\frac{\tau_i h_{\text{ref}}}{2}\frac{a_{\text{ref}}}{\mu a}\left(\frac{I}{I_{\text{ref}}}\right)^2 - \left(\frac{\partial p}{\partial X_i} - \rho g_i\right)\frac{h_{\text{ref}}^2}{3}\frac{a_{\text{ref}}^2}{\mu a^2}\left(\frac{I}{I_{\text{ref}}}\right)^3\right] = 0, \qquad (i = 1, 2) \qquad (13)$$

According to Eq. (13), the temperature effect on skin-friction measurement is mainly contained in the factors $a_{\text{ref}}/\mu a$ and $a_{\text{ref}}^2/\mu a^2$. The temperature dependencies of the luminescent quantum efficiency and oil viscosity are approximately given by $\Phi = \Phi(T_0)\exp[-C_I(T - T_0)]$ and $\mu = \mu(T_0)\exp[-C_\mu(T - T_0)]$ in a certain temperature range, respectively, where T and T_0 are temperature and reference temperature in Kelvin, respectively, and C_I and C_μ are coefficients. Interestingly, when a luminescent base coating is appropriately selected such that the factor $a_{\text{ref}}/\mu a$ could be independent of temperature, the temperature effect on skin-friction measurement can be largely canceled out even though $a_{\text{ref}}^2/\mu a^2$ cannot be constant at the same time.

In general, a relative skin-friction field is given. To determine the unknown proportional coefficient in the relative skin-friction field, in situ calibration uses some accurate values of skin friction at several locations (at least one) given by an interferometric oil-film meter (other reliable experimental, computational, and theoretical methods). This is very similar to the in situ calibration method for PSP [25]. Therefore, a global, absolute skin-friction field can be obtained using this in situ approach. In this work, the relative skin-friction field $\bar{\boldsymbol{\tau}}/g$ or normalized skin-friction field is presented without a priori or in situ calibration.

V. Measurement System

To make luminescent oil, a small quantity of luminescent material is used. In this work, europium thenoyltrifluoroacetonate (EuTTA) and high-visibility UV powders were used. EuTTA, which was purchased from Gelest, Inc., (www.gelest.com), was dissolved in a solvent (dope thinner) and then mixed with silicone oil. It was found that EuTTA tended to stick on a Mylar surface, and this could cause error in luminescence-based oil thickness measurement. High-visibility UV powders (UVHiVisOR) produced by LDP LLC (www.MaxMax.com) were also used, which are insoluble luminescent particles of about 5 μm. The resulting luminescent oil emits radiation at a longer wavelength due to the Stokes shift when illuminated by an appropriate light source like a UV lamp. At the current stage, the temperature sensitivity of the luminescent material is not a concern for low-speed flows with a constant temperature.

The camera system for a luminescent oil film is similar to that used for PSP and TSP. Figure 4 shows a typical measurement system for luminescent oil film on an airfoil model. The luminescent oil is either brushed or sprayed on a surface, and is excited to luminesce by an illumination source with a suitable wavelength (UV lamps in our tests). After the illumination light is optically filtered, a time sequence of luminescent intensity images of the developing oil film is captured using a digital camera after the tunnel starts. The measurement system used in our tests includes a charge-coupled device (CCD) video camera for imaging and UV lamps for illumination.

VI. Experiments

To demonstrate and examine the developed method, global skin-friction measurements are conducted in an oblique circular impinging jet, delta wing, and circular cylinder junction flow. Although these typical flows have been extensively studied for years, global measurements of skin-friction fields are rare. Using SSLC, Reda et al. [5,6] measured a skin-friction field in an oblique impinging jet after an intensive work of color calibration for a specific setup. Fonov et al. [9] and Crafton et al. [10] reported measurement of a skin-friction field on a delta wing using S3F. Compared with SSLC and S3F, instrumentation and test preparation for this method are much easier and simpler. In the following

experiments, a correction procedure for nonuniform illumination was not applied in data processing. Instead, UV lamps were arranged in such a way that an illumination field was roughly uniform on a flat or relatively flat surface where oil was coated.

A. Impinging Jet

To validate the proposed method, a skin-friction field on a flat wall in a low-speed, oblique circular impinging jet was measured in comparison with hot-film measurements. A jet from a circular tube nozzle with an inner diameter of 8 mm impinged on a flat plate at an inclination angle of 45 deg. The height of the exit center to the wall was 28.6 mm and the distance between the exit center and geometrical impingement point was 5.6 exit diameters. The exit velocity was 16.2 m/s, the exit flow was laminar, and the exit velocity profile was approximately parabolic. A white Mylar sheet was covered on the measurement region to enhance the luminescent emission. Dow Corning 100 cS silicone oil doped with EuTTA was brushed on the surface and two UV lamps were used to excite the oil. A CCD video camera viewing the wall perpendicularly was used to image the evolution of the luminescent oil film at 25 f/s after the jet was turned on. Figure 5 shows two typical images of the luminescent oil film in the impinging jet at 9.6 and 10 s after starting the jet. Figure 6 shows the x components of the snapshot solutions at a time sequence with a 0.4 s interval, where the negative x component of skin friction indicates the reversed flow. The arrow indicates the change of snapshot solutions as time increases. Here, the x coordinate directs in the mainstream along the projected nozzle centerline on the wall, and its origin is located at the geometrical impingement point that is the intersection between the wall and nozzle centerline. Because the image plane is parallel to the wall, the x coordinate corresponds to the vertical axis through the impingement point in the image plane. The snapshot solutions are directly superposed to reconstruct a complete relative skin-friction field. Figure 7 shows the reconstructed skin-friction vector field, which is a coarser representation of the much denser field (one vector per pixel) for the purpose of illustration.

The distribution of the normalized skin-friction magnitude along the x coordinate is shown in Fig. 8. The data are normalized by the peak value of skin-friction magnitude. The stagnation point is located at about half of the jet exit diameter upstream the geometrical impingement point. This is due to the viscous effect, and the deviation from the geometrical impingement point is consistent with the exact solution of the Navier–Stokes equations for a nonorthogonal stagnation-point flow [26,27]. For comparison, the skin-friction magnitude distribution along the centerline was also measured using a glued-on hot-film sensor, and the relative skin friction was calculated using $\tau = A(E^2 - E_0^2)^3$, where E and E_0 are the voltages with and without flow, respectively. The main features of the distributions obtained in the oil-film and hot-film measurements are consistent particularly in the mainstream. However, the hot-film sensor gives a higher value (a much smaller valley) at the stagnation point, whereas it gives a lower peak value in the reversed flow region. There are some reasons for the discrepancy. Because the classical relation $\tau = A(E^2 - E_0^2)^3$ is valid only for a linear velocity profile in a boundary layer, the quantitative accuracy of this relation is questionable near the stagnation point and in the reversed flow region with a strong adverse pressure gradient. Therefore, the hot-film measurements provide a reference here rather than a benchmark. On the other hand, the oil-film results are not accurate either near the stagnation point because the effect of pressure gradient is not taken into account in this case.

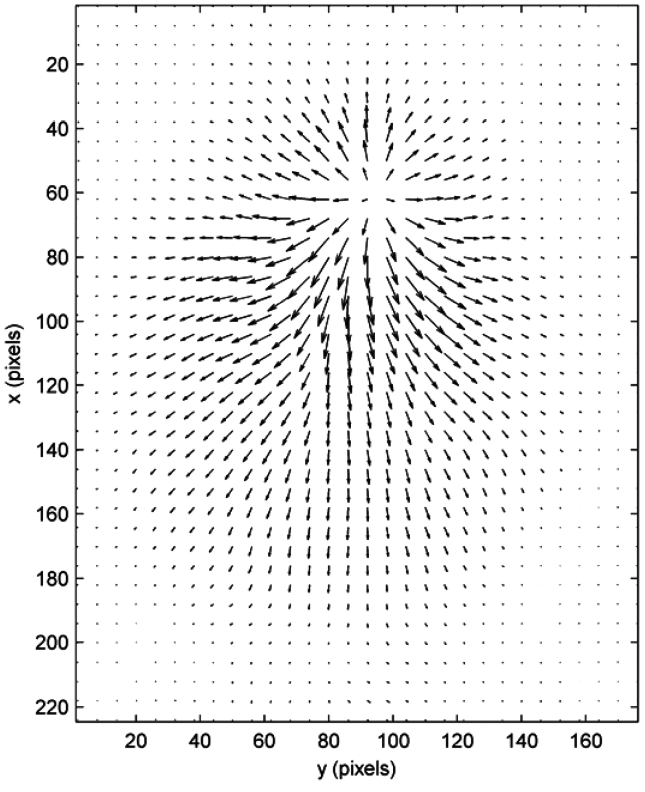

Fig. 7 Skin-friction vectors in the oblique impinging jet.

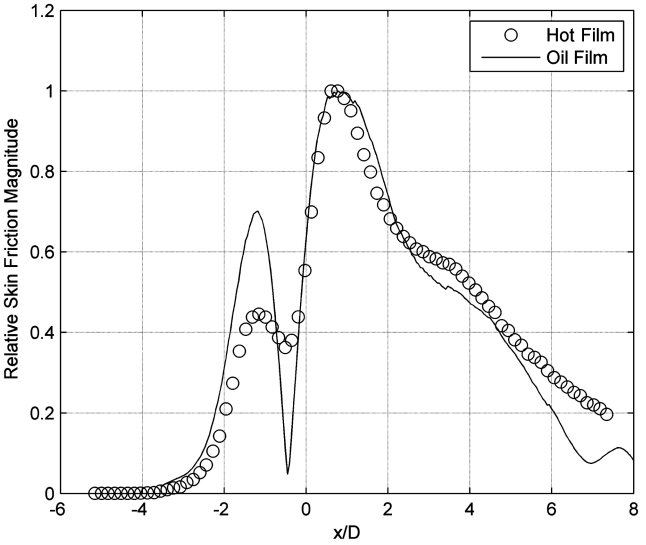

Fig. 8 Skin-friction magnitude along the x axis (projected jet centerline) in the oblique impinging jet.

B. NACA Airfoil

Skin-friction measurements on a NACA 2412 airfoil section were carried out in a low-speed wind tunnel with a test section of 16 × 16 in. at the Applied Aerodynamics Laboratory of Western Michigan University. A glass window at the top of the test section allowed optical access. The NACA 2412 airfoil section with a 12 in. chord was made of aluminum. A white Mylar sheet covered in the middle section of the airfoil for enhancing luminescent emission. Before the tunnel started, a 2-in.-wide strip of Dow Corning 200 cS silicone oil mixed with high-visibility UV powders (UVHiVisOR) was brushed on the Mylar from the leading edge to trailing edge of the airfoil. After the flow was started, the evolution of the luminescent oil strip under excitation of two UV lamps was recorded at a frame rate of 25 f/s using a digital camera viewing from the top. The freestream velocity was 16 m/s.

A total of about 30 snapshot solutions were obtained from successive image pairs with a 4 s interval between them. Figure 9 shows a typical pair of the luminescent images of the oil strip on the NACA 2412 airfoil during a run. Some nonuniform wavy features of the oil film are seen in Fig. 9. The relative skin-friction field on the strip is obtained using both the direct superposition and wavelet fusion methods for 30 snapshot solutions. For comparison, a

a)

b)

Fig. 9 Two successive images of luminescent oil stripe on a NACA 2412 airfoil section (the leading edge is on left) at a) 108 s and b) 112 s.

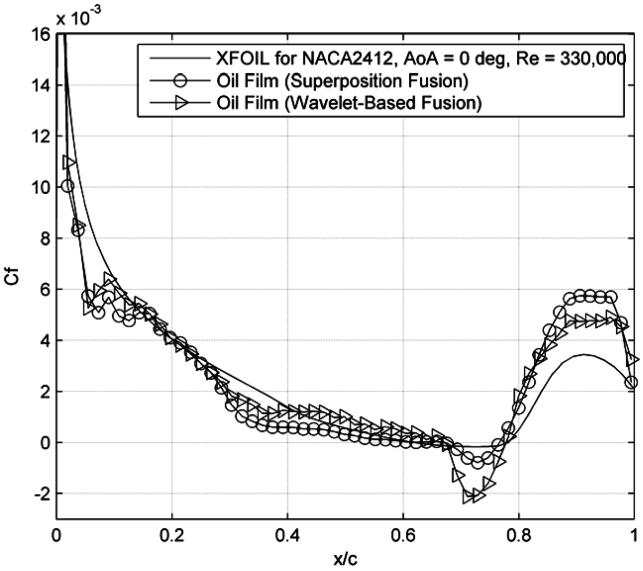

Fig. 10 Skin-friction coefficient distribution on the upper surface of a NACA 2412 airfoil section.

computational fluid dynamics (CFD) code XFOIL, which is an interactive program for the design and analysis of subsonic airfoils [28], is used to provide a reasonable prediction for skin friction in a laminar boundary layer on an airfoil at zero angle of attack (AoA). Figure 10 shows the chordwise distribution of the skin-friction coefficient C_f on the NACA 2412 airfoil at zero AoA for the Reynolds number based on the chord $Re_c = 3.3 \times 10^5$. The measured skin-friction distributions are averaged in the spanwise direction across the oil stripe. The value of C_f at 20% chord given by XFOIL is used to determine the proportional constant for in situ calibration in the oil-film measurements.

The skin-friction distributions obtained by the oil-film technique are basically consistent with one given by XFOIL in the laminar boundary layer. The direct superposition and wavelet fusion methods give approximately the same results in the laminar region. The angular effect of the luminescent emission due to the large surface curvature near the leading edge may lead to an underestimate of C_f near the leading edge, as indicated in Fig. 10. The oil-film measurements on the NACA 2412 airfoil reveal a separation bubble at 70–80% of the chord before transition. The measured skin-friction magnitude in the revered flow within the separation bubble is larger than that predicted by XFOIL, whereas the measured beginning location of the bubble approximately corresponds to the predicted one. The wavelet fusion method gives even larger skin-friction magnitudes in the separation bubble. The measured boundary-layer transition location after the separation bubble is in good agreement with the prediction by the e^N method with $N = 9$. In the turbulent region, the measured skin-friction magnitudes are larger than the prediction by XFOIL.

C. Delta Wing

Global skin-friction measurements on a delta wing with 65 deg swept angle with a chord of 13 in. and a span of 12 in. were conducted. The upper surface of the delta wing was flat and the leading-edge angle of the delta wing was 45 deg. The freestream velocity was 13 m/s and the Reynolds number based on the chord was 3×10^5. Dow Corning 200 cS silicone oil mixed with high-visibility UV powders was brushed on the white Mylar covering the upper surface of the delta wing. Figure 11a shows a typical luminescent oil-film image of the delta wing for an AoA of 13 deg. Figures 11b–11d show the normalized skin-friction vectors, skin-friction lines, and skin-friction magnitude distribution for an AoA of 13 deg. The skin-friction field is normalized by the skin-friction magnitude at 30% of the chord at the wing centerline. The reattachment line of the primary leading-edge vortices and separation line between the primary vortices and secondary vortices are clearly observed in Fig. 11c. Most experimental studies of the topological structures of flows on delta wings have been based on oil-streak visualizations [29]; such a quantitative high-resolution mapping of skin friction on a delta wing presented here has never been achieved before.

VII. Discussions on Errors and Shortcomings

In spite of the distinct advantages of this method, some error sources and shortcomings should be discussed for further improvements. Compared with interferometric oil-film measurements in which the oil-film thickness is typically on the order of the light wavelength, the oil-film thickness in luminescent oil measurements is much thicker (on the order of microns) depending on the local skin-friction magnitude. The effect of the finite thickness is particularly pronounced near critical points like nodes, saddles, and foci in complex separated flows through the terms of pressure gradient and gravity in Eq. (1). Although the effects of pressure gradient and gravity are not considered at this stage, a correction scheme for these effects near critical points should be developed to improve the accuracy of skin-friction measurements, particularly in three-dimensional separated flows. In addition, the finite oil-film thickness may slightly alter the effective geometry of a wing or body. This is a common shortcoming of all coating-based measurement techniques. This work does not correct the effect of nonuniform illumination on a surface in luminescence measurement. In principle, using a homogeneous reference luminescent coating with a distinctly different wavelength from the luminescent oil, a two-color ratioing procedure can eliminate the effect of nonuniform illumination [25]. In this paper, a simple perspective projection transformation is used to transform the thin oil-film equation from the object space to the image plane such that the data processing can be conveniently carried out in the image plane. This is only good when the image plane is approximately parallel to a flat or relatively flat measurement surface. For a highly curved surface that is viewed by a camera from a large angle, a general mapping between the surface and image plane should be used. Currently, a heuristic fusion scheme (direct superposition fusion or wavelet-based fusion) is proposed to reconstruct a complete skin-friction field from snapshot solutions. Although the heuristic fusion method is based on some plausible arguments, a rigorous foundation for fusion of snapshot solutions should be further built.

VIII. Conclusions

The global luminescent oil-film skin-friction meter is developed to extract a skin-friction field from a time sequence of images of luminescent oil film developing in flow. The innovative elements in this work are the derivation of the projected thin oil-film equation relating a skin-friction field to the oil luminescent intensity and a solution for a skin-friction field based on a variational formulation with an appropriate constraint. This method provides not only a general and rational foundation for global quantitative skin-friction diagnostics with a high spatial resolution for complex flows, but also allows easy and reliable instrumentation based on oil luminescence measurements in various facilities. Without a priori calibration, this method is able to give a relative or normalized skin-friction field. With in situ calibration, using a point-based sensor like an interferometric skin-friction meter at one or several locations, the

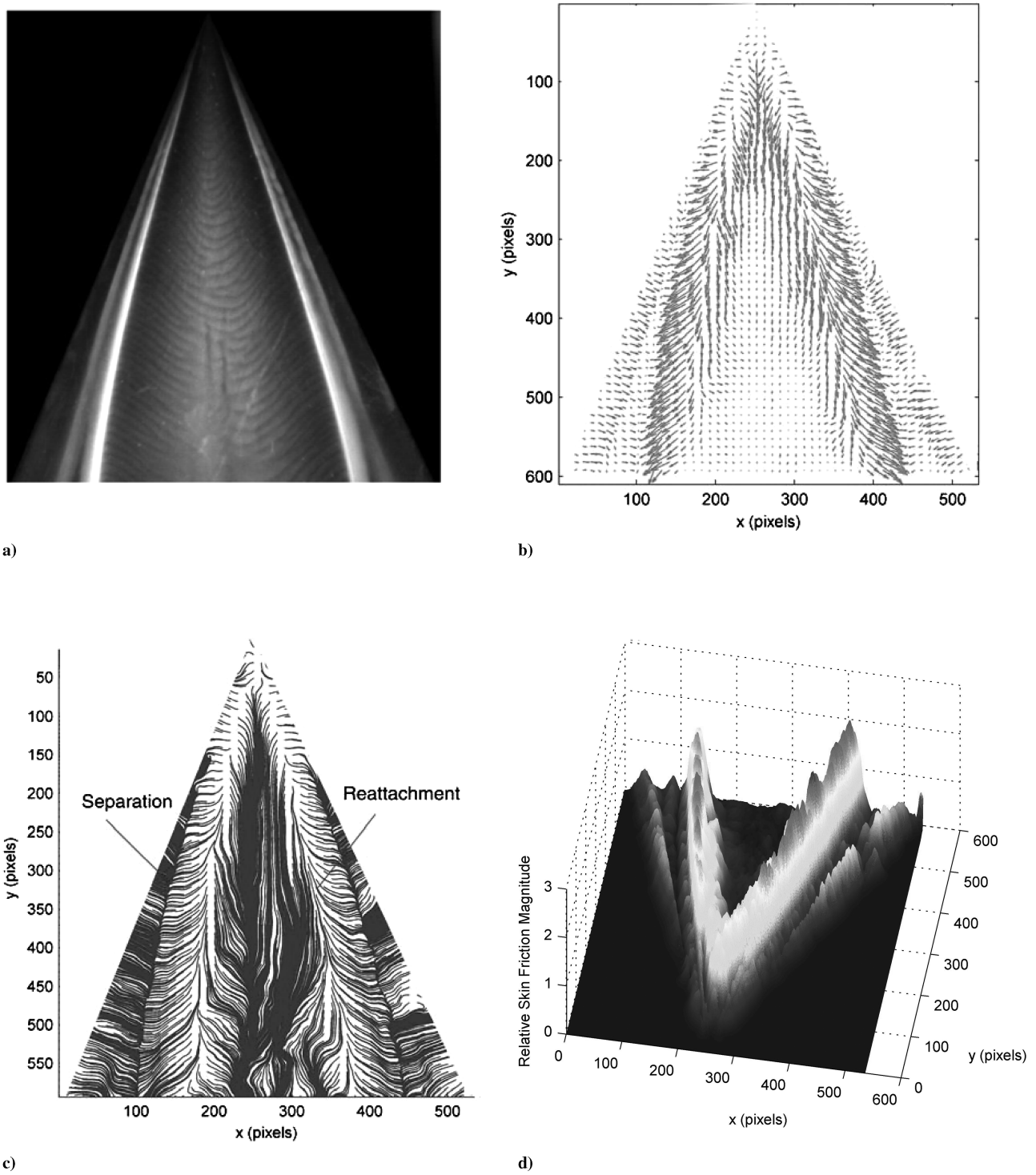

Fig. 11 Flow over a delta wing with 65 deg swept angle at AoA of 13 deg: a) typical luminescent oil image, b) skin-friction vectors, c) skin-friction lines, and d) normalized skin-friction magnitude for $Re_c = 3 \times 10^5$.

absolute skin friction can be determined. In addition, instrumentation for this method is compatible to pressure and temperature sensitive paints for unified measurements of surface pressure, temperature, and skin-friction fields.

Appendix A: Algorithm

A discrete scheme is given to solve the Euler–Lagrange equations [Eq. (8)]. For simplicity of expression, the equivalent skin friction is denoted as $\bar{\tau} = (u, v)$ in this Appendix. Let us define the following notations:

$$(\delta_x u)_{i,j} = (u_{i+1,j} - u_{i-1,j})/2, \qquad (\delta_y u)_{i,j} = (u_{i,j+1} - u_{i,j-1})/2$$

$$(\delta_{xy} u)_{i,j} = (u_{i+1,j} - u_{i+1,j-1} - u_{i-1,j+1} + u_{i-1,j-1})/4$$

$$\bar{u}^x_{i,j} = (u_{i+1,j} + u_{i-1,j})$$

$$\bar{u}_{i,j} = (u_{i+1,j} + u_{i+1,j-1} + u_{i-1,j+1} + u_{i-1,j-1})/4$$

Furthermore, $(\delta_x v)_{i,j}$, $(\delta_y v)_{i,j}$, $(\delta_{xy} v)_{i,j}$, $\bar{v}^x_{i,j}$, and $\bar{v}_{i,j}$ are similarly defined. Using these notations and the five-point discrete scheme, Eq. (8) becomes

$$
\begin{aligned}
&(gg_{xx} - 2h^{-2}g^2 - 4\alpha h^{-2})u_{i,j} + gg_{xy}v_{i,j} \\
&\quad = g(f_x - g_{xt}) - g[2g_x(\delta_x u)_{i,j} + g_y(\delta_x v)_{i,j} + g_x(\delta_y v)_{i,j}] \\
&\quad - h^{-2}g^2[\bar{u}^x_{i,j} + (\delta_{xy}v)_{i,j}] - \alpha h^{-2}\bar{u}_{i,j} \\
&gg_{xy}u_{i,j} + (gg_{yy} - 2h^{-2}g^2 - 4\alpha h^{-2})v_{i,j} \\
&\quad = g(f_y - g_{yt}) - g[2g_y(\delta_x u)_{i,j} + g_x(\delta_y u)_{i,j} + g_y(\delta_y v)_{i,j}] \\
&\quad - h^{-2}g^2[(\delta_{xy}u)_{i,j} + \bar{u}^y_{i,j}] - \alpha h^{-2}\bar{v}_{i,j} \qquad \text{(A1)}
\end{aligned}
$$

where h is the spatial step that is typically one pixel. The preceding linear system is solved using the blockwise Jacobi iterative method. More precisely, we have the following algorithm.

Step 1: Let $(u^0_{i,j}, v^0_{i,j})^T$ be an initial value and ε be the given error tolerance.

Step 2: Compute the nth iteration as follows

$$
\begin{bmatrix} u^{n+1}_{i,j} \\ v^{n+1}_{i,j} \end{bmatrix} = \boldsymbol{A}^{-1}_{i,j}\boldsymbol{b}^n_{i,j} \qquad \text{(A2)}
$$

where

$$
\boldsymbol{A}_{i,j} = \begin{bmatrix} (gg_{xx} - 2h^{-2}g^2 - 4\alpha h^{-2}) & gg_{xy} \\ gg_{xy} & (gg_{yy} - 2h^{-2}g^2 - 4\alpha h^{-2}) \end{bmatrix}
$$

$$
\begin{aligned}
\boldsymbol{b}^n_{i,j} &= g\begin{bmatrix} (f_x - g_{xt}) - [2g_x(\delta_x u^n)_{i,j} + g_y(\delta_x v^n)_{i,j} + g_x(\delta_y v^n)_{i,j}] \\ (f_y - g_{yt}) - [2g_y(\delta_x u^n)_{i,j} + g_x(\delta_y u^n)_{i,j} + g_y(\delta_y v^n)_{i,j}] \end{bmatrix} \\
&\quad - h^{-2}\begin{bmatrix} g^2[(\bar{u}^x_{i,j})^n + (\delta_{xy}v^n)_{i,j}] + \alpha(\bar{u}_{i,j})^n \\ g^2[(\delta_{xy}u^n)_{i,j} + (\bar{u}^y_{i,j})^n] + \alpha(\bar{v}_{i,j})^n \end{bmatrix}
\end{aligned}
$$

Step 3: If $\max(\|u^{n+1} - u^n\|_2, \|v^{n+1} - v^n\|_2) \le \varepsilon$, stop; otherwise, go to step 2.

Appendix B: Approximate Solution for Skin Friction

When the effects of pressure gradient and gravity are neglected, the thin oil-film equation is

$$
\frac{\partial h}{\partial t} + \frac{\partial}{\partial X_i}\left[\frac{\tau_i h^2}{2\mu}\right] = 0, \qquad (i = 1, 2) \qquad \text{(B1)}
$$

Projection of Eq. (B1) onto a skin-fraction line yields

$$
\frac{\partial h}{\partial t} + \frac{\partial}{\partial s}\left[\frac{\tau_s h^2}{2\mu}\right] + \frac{\tau_s h^2}{2\mu}\kappa n_i \frac{\partial s}{\partial X_i} = 0 \qquad \text{(B2)}
$$

where s is the arc length along a skin-friction line, $\tau_s = \boldsymbol{s}\cdot\tau$ is the skin friction along the tangential direction $\boldsymbol{s}$ of the skin-friction line, and κ and n_i are the curvature and normal of the skin-friction line, respectively. To obtain Eq. (B2), the Frenet–Serret formula $\partial s_j/\partial X_i = \kappa n_j \partial s/\partial X_i$ is used. For a small curvature, Eq. (B2) becomes

$$
\frac{\partial h}{\partial t} + \frac{\partial}{\partial s}\left[\frac{\tau_s h^2}{2\mu}\right] = 0 \qquad \text{(B3)}
$$

With the similarity variables $h/h_0 = f(\xi)$ and $\xi = \mu s/(\tau_s t h_0)$, Eq. (B3) is transformed to an semisimilar equation

$$
f(\xi) = \xi + (t/t_1)\xi - (t/t_2)f^2/f' + (s/s_1)f \qquad \text{(B4)}
$$

where the temporal and spatial scales of the oil-film evolution are defined as

$$
t_1 = \frac{\tau_s}{\partial\tau_s/\partial t} \qquad \text{(B5)}
$$

$$
t_2 = \frac{\mu}{h_0\partial\tau_s/\partial s} \qquad \text{(B6)}
$$

$$
s_1 = \frac{\tau_s}{\partial\tau_s/\partial s} \qquad \text{(B7)}
$$

For $\partial\tau_s/\partial s = 0$, $\partial\tau_s/\partial t = 0$, and $\tau_s \ne 0$, a self-similar solution $f(\xi) = \xi$ is obtained. In general, only a semisimilar solution can be obtained for the given nondimensional times and location. The thin oil-film evolution deviates from the self-similar state, depending on the two time scales and one spatial scale. Substitution of the self-similar solution $f(\xi) = \xi$ into the right-hand side of Eq. (B4) leads to a first-order approximate solution

$$
f(\xi) = \xi + (t/t_1)\xi - (t/t_2)\xi^2 + (s/s_1)\xi \qquad \text{(B8)}
$$

Differentiating Eq. (B4) with respect to s and t yields after some arrangements

$$
\begin{aligned}
\tau_s &= \mu\frac{\partial}{\partial t}\left(\frac{\partial h}{\partial s}\right)^{-1} - t\frac{\partial\tau_s}{\partial t} - \mu\frac{\partial}{\partial t}\left[\frac{s}{s_1}\left(\frac{\partial h}{\partial s}\right)^{-1}\right] \\
&\quad + \frac{\partial}{\partial t}\left[t\tau_s\left(\frac{\partial h}{\partial s}\right)^{-1}\frac{\partial G}{\partial s}\right] \qquad \text{(B9)}
\end{aligned}
$$

where $G = h_0 f(\xi)$. For $\tau_s \propto H(t)$ and $\partial\tau_s/\partial t \propto \delta(t)$, after a transient stage, a special solution is

$$
\tau_s = \mu\frac{\partial}{\partial t}\left(\frac{\partial h}{\partial s}\right)^{-1}\left(1 - \frac{s\partial\tau_s/\partial s}{\tau_s}\right) \qquad \text{(B10)}
$$

where $H(t)$ is the Heaviside function and $\delta(t)$ is the Dirac-delta function.

References

[1] Winter, K. G., "An Outline of the Techniques Available for Measurement of Skin Friction in Turbulent Boundary Layer," *Progress in Aerospace Sciences*, Vol. 18, No. 1, 1977, pp. 1–57.

[2] Settles, G. S., "Recent Skin Friction Techniques for Compressible Flows," AIAA Paper 86-1099, May 1986.

[3] Naughton, J. W., and Sheplak, M., "Modern Developments in Shear-Stress Measurement," *Progress in Aerospace Sciences*, Vol. 38, Nos. 6–7, 2002, pp. 515–570. doi:10.1016/S0376-0421(02)00031-3

[4] Plesniak, M., and Peterson, S., "Wall Shear Stress Measurements for Conventional Applications and Biomedical Flows," AIAA Paper 2004-2301, Portland, OR, June 2004.

[5] Reda, D. C., Wilder, M. C., Farina, D. J., and Zilliac, G., "New Methodology for the Measurement of Surface Shear Stress Vector Distributions," *AIAA Journal*, Vol. 35, No. 4, 1997, pp. 608–614.

[6] Reda, D. C., Wilder, M. C., Mehta, R. D., and Zilliac, G., "Measurement of Continuous Pressure and Shear Distributions Using Coating and Imaging Techniques," *AIAA Journal*, Vol. 36, No. 6, 1998, pp. 895–899.

[7] Reda, D. C., and Wilder, M. C., "Shear-Sensitive Liquid Crystal Coating Method Applied Through Transparent Test Surfaces," *AIAA Journal*, Vol. 39, No. 1, 2001, pp. 195–197.

[8] Buttsworth, D. R., Elston, S. J., and Jones, T. V., "Directional Sensitivity of Skin Friction Measurements Using Nematics Liquid Crystal," *Measurement Science and Technology*, Vol. 9, No. 11, 1998, pp. 1856–1865. doi:10.1088/0957-0233/9/11/011

[9] Fonov, S. D., Jones, G., Crafton, J., Fonov, V., and Goss, L., "The Development of Optical Technique for the Measurement of Pressure and Skin Friction," *Measurement Science and Technology*, Vol. 17, No. 6, 2006, pp. 1261–1268. doi:10.1088/0957-0233/17/6/S05

[10] Crafton, J. W., Fonov, S. D., Jones, G., and Fonov, V. S., "Optical Measurements of Pressure and Shear in a Plasma," AIAA Paper 2005-5006, June 2005.

[11] Tanner, L. H., and Blows, L. G., "A Study of the Motion of Oil Films on Surfaces in Air Flow, with Application to the Measurement of Skin Friction," *Journal of Physics E: Scientific Instruments*, Vol. 9, No. 3, 1976, pp. 194–202. doi:10.1088/0022-3735/9/3/015

[12] Monson, D. J., and Higuchi, H., "Skin Friction Measurements by a Dual-Laser-Beam Interferometer Technique," *AIAA Journal*, Vol. 19, No. 6, 1981, pp. 739–744.

[13] Kim, K. S., and Settles, G. S., "Skin Friction Measurements by Laser Interferometry in Swept Shock/Boundary-Layer Interactions," *AIAA Journal*, Vol. 28, No. 1, 1990, pp. 133–139.
[14] Monson, D. J., Mateer, G. G., and Menter, F. R., "Boundary-Layer and Global Skin Friction Measurement with an Oil-Fringe Imaging Technique," *SAE Aerotech '93*, Society of Automotive Engineers Paper No. 932550, Sept. 1993.
[15] Naughton, J. W., and Brown, J. L., "Surface Interferometric Skin-Friction Measurement Technique," AIAA Paper 96-2183, June 1996.
[16] Zilliac, G. G., "Further Development of the Fringe-Imaging Skin Friction Technique," NASA TM 110425, Dec. 1996.
[17] Brown, J. L., and Naughton, J. W., "The Thin Oil Film Equation," NASA TM 1999-208767, March 1999.
[18] Liu, T., and Sullivan, J. P., "Luminescent Oil-Film Skin Friction Meter," *AIAA Journal*, Vol. 36, No. 8, 1998, pp. 1460–1465.
[19] Liu, T., "Geometric and Kinematic Aspects of Image-Based Measurements of Deformable Bodies," *AIAA Journal*, Vol. 42, No. 9, 2004, pp. 1910–1920.
[20] Liu, T., and Shen, L., "Determination of Velocity and Skin Friction Fields from Images by Solving Projected Motion Equations," *22nd International Congress on Instrumentation in Aerospace Simulation Facilities (ICIASF)*, International Congress on Instrumentation in Aerospace Simulation Facilities, Pacific Grove, CA, June 2007.
[21] Horn, B. K., and Schunck, B. G., "Determining Optical Flow," *Artificial Intelligence*, Vol. 17, Nos. 1–3, 1981, pp. 185–204. doi:10.1016/0004-3702(81)90024-2
[22] Barenblatt, G. I., *Scaling, Self-Similarity, and Intermediate Asymptotics*, Cambridge Univ. Press, Cambridge, England, U.K., 1996.
[23] Daubechies, I., *Ten Lectures on Wavelets*, CBMS Conference Series in Applied Mathematics, Vol. 61, Society for Industrial and Applied Mathematics, Philadelphia, 1992, Chap. 8.
[24] Cohen, A., Daubechies, I., and Feauveau, J., "Biorthogonal Bases of Compactly Supported Wavelets," *Communications on Pure and Applied Mathematics*, Vol. 45, No. 5, 1992, pp. 485–500. doi:10.1002/cpa.3160450502
[25] Liu, T., and Sullivan, J. P., *Pressure and Temperature Sensitive Paints (Experimental Fluid Mechanics)*, Springer–Verlag, Berlin, 2004, Chap. 3.
[26] Dorrepaal, J. M., "An Exact Solution of the Navier–Stokes Equation Which Describes Non-Orthogonal Stagnation-Point Flow in Two Dimensions," *Journal of Fluid Mechanics*, Vol. 163, Feb. 1986, pp. 141–147. doi:10.1017/S0022112086002240
[27] Liu, T., "Non-Orthogonal Stagnation Flow on the Surface of a Quiescent Fluid: An Exact Solution of the Navier–Stokes Equation," *Quarterly of Applied Mathematics*, Vol. L, No. 1, 1992, pp. 39–47.
[28] Drela, M., "XFOIL: An Analysis and Design System for Low Reynolds Number Airfoil," *Conference on Low Reynolds Number Airfoil Aerodynamics*, University of Notre Dame, South Bend, IN, June 1989.
[29] Tobak, M., and Peake, D. J., "Topology of Three-Dimensional Separation Flows," *Annual Review of Fluid Mechanics*, Vol. 14, Jan. 1982, pp. 61–85. doi:10.1146/annurev.fl.14.010182.000425

F. Coton
Associate Editor